Atmos. Chem. Phys. Discuss., 10, 25841–25869, 2010
www.atmos-chem-phys-discuss.net/10/25841/2010/
doi:10.5194/acpd-10-25841-2010


Atmospheric Chemistry and Physics Discussions



# Characterization of submicron aerosols at a rural site in Pearl River Delta of China using an Aerodyne High-Resolution Aerosol Mass Spectrometer

**X.-F. Huang[1], L.-Y. He[1], M. Hu[2], M. R. Canagaratna[3], J. H. Kroll[4], N. L. Ng[3], Y.-H. Zhang[2], Y. Lin[1], L. Xue[1], T.-L. Sun[1], X.-G. Liu[2], M. Shao[2], J. T. Jayne[3], and D. R. Worsnop[3]**

[1]Key Laboratory for Urban Habitat Environmental Science and Technology, School of Environment and Energy, Peking University Shenzhen Graduate School, Shenzhen, China
[2]State Key Joint Laboratory of Environmental Simulation and Pollution Control, College of Environmental Sciences and Engineering, Peking University, Beijing, China
[3]Aerodyne Research, Inc. Billerica, MA, USA







[4]Department of Civil and Environmental Engineering, Massachusetts Institute of Technology, Cambridge, MA, USA

Received: 21 October 2010 – Accepted: 28 October 2010 – Published: 3 November 2010

Correspondence to: L.-Y. He (hely@pku.edu.cn)

Published by Copernicus Publications on behalf of the European Geosciences Union.







## Abstract

The Pearl River Delta (PRD) region in South China is one of the most economically developed regions in China, but it is also noted for its severe air pollution due to industrial/metropolitan emissions. In order to continuously improve the understanding and quantification of air pollution in this region, an intensive campaign was executed in PRD during October–November 2008. Here, we report and analyze Aerodyne High-Resolution Aerosol Mass Spectrometer measurements at Kaiping, a rural site downwind of the highly-polluted central PRD area, to characterize the general features of submicron particulate pollution in the regional air. The mean measured $PM_1$ mass concentration was $33.1 \pm 18.1\,\mu g\,m^{-3}$ during the campaign and composed of organic matter (33.8%), sulfate (33.7%), ammonium (14.0%), nitrate (10.7%), black carbon (6.7%), and chloride (1.1%), which is characterized by high fractions of inorganic ions due to huge emissions of $SO_2$ and $NO_x$ in PRD. The average size distributions of the species (except BC) were all dominated by an accumulation mode peaking at ~450 nm in vacuum aerodynamic diameter. Calculations based on high-resolution organic mass spectra indicate that C, H, O, and N on average contributed 56.6, 7.0, 35.1, and 1.3% to the total organic mass, respectively, corresponding to an organic matter mass to organic carbon mass ratio (OM/OC) of $1.77 \pm 0.08$. Based on the high-resolution organic mass spectral dataset observed, Positive Matrix Factorization (PMF) analysis differentiated the organic aerosol into three components, i.e., biomass burning (BBOA) and two oxygenated (LV-OOA and SV-OOA) organic aerosols, which on average accounted for 24.5, 39.6 and 35.8% of the total organic mass,, respectively. The BBOA showed strong features of biomass burning emissions and has been mainly attributed to field rice straw burning after harvest. The LV-OOA and SV-OOA were found to correspond to more aged (and thus less-volatile) and fresher (and semi-volatile) secondary organic aerosol, respectively. Analysis of meteorological influence supported that regional transport from the central PRD area was the major origin of the $PM_1$ components observed at the Kaiping site.






ACPD
10, 25841–25869, 2010



## 1 Introduction

The Pearl River Delta (PRD) region lies in the southeastern coastal part of China and is noted for its flourishing manufacturing and export industries. The urbanization in PRD is now characterized by several big cities like Guangzhou, Shenzhen, and Hong Kong and many medium-small cities linked by dense highways. The rapid economic development and urbanization in PRD in the recent decades comes with the consequence of severe deterioration of its atmospheric environment from urban to regional scale. For example, the annual mean $PM_{2.5}$ concentrations were reported to range from 29 (for regional background site) to 71 (for urban site) $\mu g\,m^{-3}$ in PRD with organic matter and sulfate as the most abundant constituents (Hagler et al., 2006). The air pollution problems in PRD have been a major concern of the China national government and have raised global scientific interest (Streets et al., 2006; Zhang et al., 2008).

To characterize in depth the pollution mechanisms and atmospheric chemical and radiative processes in PRD, the "Program of Regional Integrated Experiments of Air Quality over Pear River Delta (PRIDE-PRD)", sponsored by Ministry of Science and Technology, China, and developed by Peking University in collaboration with many internationally renowned institutes, conducted two intensive monitoring campaigns in October–November, 2004 and in July, 2006, respectively, which have improved much understanding on the features and environmental effects of the regional air pollution in PRD (e.g., Zhang et al., 2008; Hua et al., 2008). Built upon the PRIDE-PRD campaigns, a new intensive monitoring campaign supported by the project "Synthesized Prevention Techniques for Air Pollution Complex and Integrated Demonstration in Key City-Cluster Region" also launched by the Ministry of Science and Technology, China, was organized in PRD in October–November 2008 (STAR2008 PRD campaign) to obtain more in-situ data to test and validate the main conclusions derived from the previous campaigns. Moreover, in the STAR2008 PRD campaign, better observational framework was designed and new advanced instruments were involved, such as an Aerodyne High-Resolution Aerosol Mass Spectrometer. As part of the STAR2008 PRD





ACPD
10, 25841–25869, 2010



campaign, this paper reports the highly time-resolved High-Resolution Aerosol Mass Spectrometer measurement results for submicron aerosol particles downwind of the most polluted central PRD area, in order to better characterize the particulate pollution features in the well mixed and more aged regional air.

## 2 Experimental methods

### 2.1 Sampling site description

The landscape of PRD consists of a flat plain between the Nan Ling Mountains in the North and the South China Sea in the south. Hills surround PRD in the east, west, and north. In the STAR2008 PRD campaign, air monitoring sites were set along the northeast-southwest axis of PRD, as shown in Fig. 1, including two supersites in the rural areas, i.e., Conghua and Kaiping, respectively. In the period of October–November, under the influence of the East Asian monsoon, the prevailing wind in PRD is northeasterly and thus Conghua is upwind of the central PRD area (i.e., Guangzhou-Foshan city cluster), while Kaiping is downwind of the central PRD area, receiving pollutants through regional transport. The Kaiping supersite was located at a patriotic educational base (22.32° N, 112.53° E), about 120 km away from Guangzhou City. This site was surrounded by shrubs and eucalyptus forest and was free of any significant local pollution emissions.

### 2.2 HR-ToF-AMS operation

An Aerodyne High-Resolution Time-of-Flight Aerosol Mass Spectrometer (HR-ToF-AMS) was deployed in an air monitoring container settled at the Kaiping supersite from 12 October to 18 November 2008. A detailed instrumental description of HR-ToF-AMS can be found in DeCarlo et al. (2006). A $PM_{2.5}$ cyclone inlet was supported on the roof of the container to remove coarse particles and introduce air stream into the container





ACPD
10, 25841–25869, 2010



through a copper tube with a flow rate of 10 l $min^{-1}$. The HR-ToF-AMS sampled isokinetically from the center of the copper tube at a flow rate of 80 cc $min^{-1}$. During the campaign, the HR-ToF-AMS operated in a cycle of 5 modes every 10 min, including: 2 min V-mode to obtain the mass concentrations of the non-refractory species; 2 min W-mode to obtain high resolution mass spectral data; 4 min separate PToF (particle time-of-flight) mode to determine size distributions of species under the V-mode; and 2 min Soft-EI mode using a lower EI voltage (~13 eV). The PToF mode was not run under the W-mode because of poor signal-to-noise. The Soft-EI mode data are not included in this paper. The HR-ToF-AMS was calibrated for inlet flow, ionization efficiency (IE), and particle sizing at the beginning, the middle and the end of the campaign following the standard protocols (Jayne et al., 2000; Jimenez et al., 2003; Drewnick et al., 2005). The calibration of IE used size-selected pure ammonium nitrate particles and the particle size calibration was conducted using mono-disperse polystyrene latex spheres (PSL, density = 1.05 g $cm^{-3}$) (Duke Scientific, Palo Alto, California, USA) with nominal diameters of 100–700 nm. For a better mass closure measurement of fine particles in the campaign, a Multi-Angle Absorption Photometer (MAAP, Model 5012, Thermo) was used for simultaneous measurement of refractory black carbon (BC), which cannot be detected by HR-ToF-AMS.

### 2.3 HR-ToF-AMS data processing

Mass concentrations and size distributions of the species measured with the HR-ToF-AMS were calculated using methods outlined in DeCarlo et al. (2006). Standard ToF-AMS data analysis software packages (SQUIRREL version 1.49 and PIKA version 1.08) downloaded from the ToF-AMS-Resources webpage (http://cires.colorado.edu/jimenez-group/ToFAMSResources/ToFSoftware/index.html) were used to generate unit and high-resolution mass spectra from the V-mode and W-mode data, respectively. For mass concentration calculations an empirical particle collection efficiency (CE) factor of 0.5 was used to account for the incomplete detection of species due to





ACPD
10, 25841–25869, 2010



particle bouncing at the vaporizer and partial transmission through the aerodynamic lens (Canagaratna et al., 2007). The relative ionization efficiency (RIE) values used in this study were 1.2 for sulfate, 1.1 for nitrate, 1.3 for chloride and 1.4 for organics (Jimenez et al., 2003, Canagaratna et al., 2007). A RIE value of 4.0–4.4 was used for ammonium based on the measurement of pure $NH_4NO_3$ particles.

Positive matrix factorization (PMF) (Paatero and Tapper, 1994) analysis was conducted on the high-resolution (HR) mass spectra (*m/z* 12–150) using the PMF evaluation tool developed by Ulbrich et al. (2009). Compared with unit mass-resolution (UMR) spectra, HR mass spectra can provide better separation of different organic components in PMF analysis (Docherty et al., 2008; Aiken et al., 2009, DeCarlo et al., 2010; Huang et al., 2010). The data and noise matrices input into the PMF analysis were generated with the default fragmentation waves in PIKA version 1.08. The noise values were calculated as the sum of electronic and Poisson ion-counting errors for the relevant high resolution ion fragment (Allan et al., 2003, Ulbrich et al., 2009), and those of $CO_2^+$-related ions at *m/z* 16, 17, 18, 28, and 44 were artificially increased (down-weighted) according to the procedure discussed by Ulbrich et al. (2009). Weak ions (0.2<signal to noise ratio<2) were downweighted by a factor of 3 while bad ions (signal to noise ratio<0.2) were removed from the analysis (Paatero and Hopke, 2003; Ulbrich et al., 2009). The average noise value observed for ions during low signal time periods was used as the minimum error value for the error matrix. More technical details of the PMF analysis can be found in another of our recent publication (Huang et al., 2010). Elemental analysis of the organic components identified by PMF was carried out with the methods described previously (Aiken et al., 2007, 2008).





ACPD
10, 25841–25869, 2010



## 3 Results and discussion

### 3.1 Variations of $PM_1$ components

During the entire campaign from 12 October to 18 November 2008, the average ambient temperature and relative humidity at the Kaiping site were 24 ± 5 °C and 69 ± 15%, respectively, as shown in Fig. 2a. A clear diurnal pattern of wind during the campaign can be observed in Fig. 2b: east-northeasterly wind usually blew during the day, bringing pollution from the central PRD area to Kaiping, while during the night the wind usually became calm. An exception, however, was that during 8–10 November a cold front passed through PRD, which was characterized by continuous lower temperature and stronger east-northeasterly wind. There were few rainfall events during the campaign that leaded to significant wet removal of air pollutants. These meteorological conditions were very typical of the fall in PRD.

Figure 2cẽ present the time series of the $PM_1$ mass concentration (the sum of all components measured) and of $PM_1$ components during the campaign. The corresponding statistical values of the concentrations are summarized in Table S-1. During the entire campaign, the $PM_1$ mass concentration was observed to be in a range of 2.4~150 $\mu g\,m^{-3}$, with a mean value of 33.1 $\mu g\,m^{-3}$. The $PM_1$ variation traced closely ($R^2 = 0.86$) the particle volume variation measured with a collocated Scanning Mobility Particle Sizer (SMPS, TSI Inc.) and calculated based on the size distribution between 15 and 600 nm in mobility diameter by assuming spherical particles. The mass concentrations of $PM_1$ components also varied widely. On average, organics and sulfate had equal concentrations of 11.2 $\mu g\,m^{-3}$ and together accounted for 67.5% of the $PM_1$ mass (in Fig. 2f). Ammonium, nitrate, BC, and chloride accounted for the rest 14.0, 10.7, 6.7, and 1.1% of the $PM_1$ mass, respectively. During the cold front event (8$\tilde{1}$0 November), the concentrations of all $PM_1$ species showed continuous lower concentrations as a result of higher wind speeds. After this cold front event, the meteorological conditions became back to normal and the $PM_1$ species concentrations became





ACPD
10, 25841–25869, 2010



back to higher levels. In addition, it is clearly seen that organics reached and maintained at abnormally high concentration levels (even >50 μg/m$^3$) after 12 November. A primary explanation for this high organic aerosol episode is that rice straw burning became prevalent in PRD after the rice harvest starting in mid November. More detailed analysis of contribution of biomass burning aerosol to organic aerosol is performed in Sect. 3.4.

Despite being a rural site, the average non-refractory $PM_1$ (NR-$PM_1$) mass concentration (30.9 μg m$^{-3}$, without BC) at Kaiping is much higher than those observed in the atmospheres in developed countries (below 20 μg m$^{-3}$), including at five similar urban downwind sites in UK, US, and Germany (mostly below 10 μg m$^{-3}$) (Zhang et al., 2007), as shown in Fig. 2g. In terms of NR-$PM_1$ components, Kaiping had a far higher concentration level for sulfate due to coal burning, which is still the primary energy source in China. On the other hand, the average NR-$PM_1$ mass concentration at Kaiping is about only half of that in urban Beijing in summer (61 μg m$^{-3}$) (Huang et al., 2010).

Figure 2h presents the average species size distributions determined by the HR-ToF-AMS during the campaign. All the species generally showed a similar accumulation mode peaking at a large size of ~450 nm, which is indicative of aged regional aerosol (Allan et al., 2003; Alfarra et al., 2004; Zhang et al., 2005c). Their similar size distribution patterns suggest that most of them were likely internally mixed through gas-to-particle condensation processes during aging of the air mass, which is consistent with the fact that Kaiping was a downwind rural monitoring site. Organics showed some additional mass distribution at smaller sizes of 100~300 nm, suggesting significant input of fresh primary organic aerosols. In the case of this campaign, biomass burning aerosol is implied to be a major contributor to the organic mass at smaller sizes as analyzed in Sect. 3.4. To support this hypothesis, the mean OA size distributions during biomass burning period (after 12 November) and non-biomass burning period (before 12 November) are compared in Fig. 2i. It is clearly seen that the peak of the OA size distribution moved from 450 nm to 350 nm for the biomass burning period. The difference between them yielded an OA size distribution peaking at ~300 nm, as shown





ACPD
10, 25841–25869, 2010



in Fig. 2i, more clearly indicating the contribution from fresh emissions.

### 3.2 Diurnal patterns of $PM_1$ components

Figure 3 presents the diurnal variation patterns of different $PM_1$ species in the form of box plot. In terms of the average cases, the $PM_1$ species roughly exhibited two types of patterns: sulfate, ammonium and organics showed relatively stable concentrations during the whole day; while nitrate, chloride and black carbon showed significantly lower concentrations in the daytime. The higher planetary boundary layer (PBL) and wind speeds in the daytime should be crucial factors leading to effective dilution of air pollutants, and the semi-volatility of nitrate and chloride would further lower their daytime concentrations due to evaporation at higher temperatures (Zhang et al., 2005b; Salcedo et al., 2006; Hennigan et al., 2008; Zheng et al., 2008). The lowest concentrations of nitrate in the afternoon also suggest that the amount of its photochemical production could not overwhelm the simultaneous evaporation and dilution effects. For less-volatile secondary sulfate, its daytime photochemical production might compensate the daytime dilution effect and made its concentration level relatively stable during the whole day. The diurnal variation of ammonium is a combined result of particulate $(NH_4)_2SO_4$ and $NH_4NO_3$. As aerosol organic matter has both large primary and secondary sources and also large amounts of semi-volatile compounds, the observed diurnal variation of organics was a complex outcome of those of different types of organics, which will be provided and discussed in the next section. It is interesting to note that in the BC diurnal pattern there was an absence of a morning peak due to rush-hour traffic and a low boundary layer in the morning, which has been observed in many previous studies (Lin et al., 2009; Han et al., 2009; Aiken et al., 2009). The missing of the morning BC peak, however, is well consistent with the fact that Kaiping is free of large local traffic emissions.





ACPD
10, 25841–25869, 2010



### 3.3 Elemental composition of organic aerosol

The high-resolution organic mass spectral dataset obtained are used to calculate the elemental composition and OM/OC (the ratio of organic mass/organic carbon mass) of organic aerosols following the methods described previously (Aiken et al., 2007, 2008). Figure 4a and b show the variations of the atomic ratios of H/C, N/C and O/C and the mass ratio of OM/OC of organic aerosols during this campaign. On average, C, H, O, and N contributed 56.6, 7.0, 35.1, and 1.3% to the total organic mass, respectively, as shown in Fig. 4c. The H/C ratio varies in a range of 1.26∼1.69, with a mean value of $1.48 \pm 0.08$, while the O/C ratio varies in a range of 0.19∼0.78, with a mean value of $0.47 \pm 0.07$. The O/C ratio is regarded as a good reference for oxidation state and photochemical age of organic aerosols (Jimenez et al., 2009; Ng et al., 2010), and thus the variation of O/C in this campaign roughly reflects the variation of the aging level of organic aerosol at Kaiping. The N/C ratio ranges between 0.008 and 0.036, with a mean value of $0.02 \pm 0.01$. A notable feature for the N/C variation is its continuous elevation to about 0.03 near the end of the campaign, i.e., during the biomass burning period, indicating significant input of high N-containing organic aerosols. Since the direct HR-ToF-AMS measurement of plumes from rice straw and other biomass burning in laboratory by our group did not find N/C ratios of above 0.02 (He et al., 2010), the high N/C ratios observed near the end of the campaign are inferred to be possibly due to secondary reactions involving $NH_3$ and $NO_x$ in biomass burning plume and/or simultaneous burning of high N-containing soil material in the open field. Figure 4d shows a Van Krevelen diagram (H/C versus O/C of organic aerosol) and an apparent anti-correlation with a slope of −0.76 was observed. This slope is shallower than those (∼1.0) ever observed in Riverside, the Central Amazon Basin, and Mexico City (Heald et al., 2010), indicating that the chemical evolution of bulk organic aerosol in the atmosphere of PRD might be somewhat different from that observed in those places. The OM/OC ratio highly correlates with the O/C ratio ($R^2 = 0.98$), having a mean value of $1.77 \pm 0.08$, which is extensively used to covert organic carbon mass to organic matter





ACPD
10, 25841–25869, 2010



mass in filter-based aerosol chemistry studies.

Figure 4e and f present the average diurnal variations of H/C, N/C, O/C and OM/OC. The O/C and OM/OC show identical diurnal patterns with the highest values in the afternoon and the lowest values in the evening. The H/C ratio show a reverse diurnal pattern to those of O/C and OM/OC as expected. Since the ratios are influenced by relative organic constitutions rather than absolute organic concentrations, their diurnal patterns should be mostly attributed to the diurnal changing of primary emissions and/or secondary production. The O/C ratio reached maximum in the early afternoon when photochemistry is the most active to produce secondary organic aerosol (SOA) with high O/C (see Sect. 3.4 for more detailed discussion of organic composition). As shown in Fig. S-1, the relative intensity of N-containing organic fragments significantly increased during biomass burning periods. The diurnal pattern of N/C showed a large peak in the late afternoon, which was possibly a result of the continuous accumulation of biomass burning-related aerosol in the atmosphere due to the daytime burning events.

### 3.4 PMF analysis of organic matter composition

The PMF analysis based on the high-resolution mass spectrum dataset observed in the campaign was performed for 1 to 8 factors, and the results and diagnostics are summarized in Table S-2. It can be seen in the table that, PMF solutions with factor numbers greater than 3 resulted in splitting behavior of the existing factors, but provided no new distinct factors. Based on all the qualified tests in Table S-2, the three factor, F peak = 0, Seed = 0 solution was chosen as the optimal solution for this analysis. The three organic components identified in this campaign include a biomass burning (BBOA) and two oxygenated (SV-OOA and LV-OOA) organic aerosol components. Figure 5 shows the MS profiles of the three components and Fig. 6a–c present their time series during the campaign. The BBOA, LV-OOA and SV-OOA on average accounted for 24.5, 39.6 and 35.8% of the total organic mass, respectively, as shown in Fig. 6d. The representativeness of the different components identified will be examined for their MS signatures,





ACPD
10, 25841–25869, 2010



correlation with tracers, and other characteristics in the following (Zhang et al., 2005c; Ulbrich et al., 2009).

The BBOA MS has an O/C ratio of 0.27 and is distinguished by a prominent contribution of *m/z* 60, which is a good tracer ion for biomass burning-emitted aerosols (Alfarra et al., 2007; Aiken et al., 2009). The O/C ratio of the BBOA is similar to those (0.18~0.26) measured for laboratory-produced different primary biomass burning organic aerosols by our group, and the HR-MS of BBOA also showed high correlations with those of the primary OAs ($R^2 = 0.67$~$0.75$) (He et al., 2010). The O/C ratio of the BBOA is also similar to that (0.30) of the BBOA identified in a similar PMF study of the AMS dataset measured in Mexico City (Aiken et al., 2009). In the PMF-resolved time series of BBOA, as shown in Fig. 6a, the large elevation of the BBOA concentration after 12 November (ave. 9.12 $\mu g\,m^{-3}$ compared to ave. 1.36 $\mu g\,m^{-3}$ before 12 November) is consistent with the fact that biomass burning smoke could be easily smelled at the sampling site during that time. The identification of BBOA in this campaign was an expected result because there are extensive farmlands around the Kaiping site and the farmers in PRD have the habit to burn off rice straw after the rice harvest around mid November. The time series of BBOA is compared to that of the collocated measurement of acetonitrile (in Fig. 6a), a well-known gaseous tracer for biomass burning emissions (de Gouw et al., 2003), using a Proton Transfer Reaction Mass Spectrometry (PTR-MS) (Yuan et al., 2010). The correlation between BBOA and acetonitrile ($R^2 = 0.60$) is consistent with the interpretation that this component has a biomass burning source. Correlation between BC and BBOA ($R^2 = 0.49$) and between BC and acetonitrile ($R^2 = 0.46$) further indicate that biomass burning was an important source of BC at Kaiping. Due to the intensive burnings after 12 November, the mean loadings of organics and BC in $PM_1$ increased by 133% and 74%, respectively, compared to the previous non-burning days, as indicated in Fig. 2d.

The MS of the two OOA components had O/C ratios of 0.64 and 0.39, respectively, and were both characterized by prominent $C_xH_yO_z$ fragments, especially $CO_2^+$ (*m/z* 44), suggesting large presence of oxidized organic compounds. OOAs have been





ACPD
10, 25841–25869, 2010



extensively identified in previous factor analyses of AMS ambient aerosol datasets and shown to be a good surrogate of secondary organic aerosol (SOA) (Zhang et al., 2005c, 2007; Jimenez et al., 2009; Ng et al., 2010). Two types of OOAs with different O/C ratios have been observed in many places from urban, suburban, to rural ambient: the OOA with higher O/C, which is more oxidized and aged, is referred to as low-volatility OOA (LV-OOA); while the OOA with lower O/C, which is less oxidized and fresher, is referred to as semi-volatile OOA (SV-OOA) (Jimenez et al., 2009; Ng et al., 2010). OOA time trends typically correlate well with those of inorganic secondary aerosol species, with LV-OOA correlating best with nitrate due to the common semi-volatility and SV-OOA correlating best with sulfate due to the common low volatility (Docherty et al., 2008; Huffman et al., 2009; Jimenez et al., 2009; Ng et al., 2010). Based on the summarization of O/C ratio ranges of OOAs revealed in global AMS measurements, Ng et al. (2010) have shown a wide range of O/C ratio for both LV-OOA ($0.73 \pm 0.14$) and SV-OOA ($0.35 \pm 0.14$), reflecting the fact that there is a continuum of OOA properties in ambient aerosols. The O/C ratios of the two OOA components identified in this campaign lie within the typical ranges for LV-OOA and SV-OOA, therefore they are referred to as LV-OOA and SV-OOA, respectively, following the existing terminology. In this campaign, the LV-OOA correlated best with sulfate ($R^2 = 0.42$) rather than with nitrate ($R^2 = 0.13$) while the SV-OOA correlated best with nitrate ($R^2 = 0.65$) rather than with sulfate ($R^2 = 0.30$), well consistent with the findings of some previous AMS measurements (Lanz et al., 2007; Docherty et al., 2008; Ulbrich et al., 2009, Huffman et al., 2009). When considering LV-OOA and SV-OOA together, the sum of them showed a quite high correlation with the sum of sulfate and nitrate ($R^2 = 0.78$), further confirming their secondary nature of OOA.

It is interesting to note that a hydrocarbon-like (HOA) organic aerosol component, typically distinguished by the ion series of $C_nH^+_{2n+1}$ and $C_nH^+_{2n-1}$ and low O/C ratios of <0.2 (Jimenez et al., 2009; Ng et al., 2010), is not identified in this PMF analysis. HOA has been extensively identified in previous AMS measurements and is mainly attributed to primary combustion sources (Zhang et al., 2007; Lanz et al., 2007; Ulbrich





ACPD
10, 25841–25869, 2010



et al., 2009). In this PMF analysis, increasing the number of PMF factors only resulted in splitting of the OOA components, as shown in Table S-2, and did not yield a new HOA-like component. The fact that a distinct HOA component was not extracted for this campaign is a result of Kaiping being a rural site about 120 km away downwind of the central PRD area. Previous studies have shown a sharp reduction in the HOA contribution to total organic aerosol loadings downwind of cities. As illustrated in Zhang et al. (2007), de Gouw et al. (2005), and Jimenez et al. (2009), HOA emitted from cities can be quickly diluted in regional air dominated by OOA and overwhelmed by SOA production. In addition, the HOA from the central PRD area could be oxidized quickly during transport because the atmospheric oxidizing capacity in PRD was demonstrated to be unexpectedly high (Hofzumahaus et al., 2009). Very small contributions of HOA to total organic aerosol mass were identified at two similar urban downwind sites, i.e., Taunus, Germany and off New England coast, US, in previous AMS measurements and no HOA was identified in analyses of data from other remote sites (Jimenez et al., 2009).

As shown in Fig. 6e, the average diurnal patterns of the three OA components are also quite different and well consistent with their own origins. The BBOA showed a small morning peak and a large evening peak, which is similar to that of acetonitrile. This type of diurnal pattern could be reasonably attributed to the combined result of the low PBL heights and burning events in the morning and evening. The LV-OOA showed a continuous concentration increase in the daytime, reflecting its large photochemical production in the daytime. As LV-OOA is regarded as aged aerosol, it is inferred to be well mixed in PBL. Therefore, unlike the near-ground emissions, the elevation of PBL in the daytime might not have a strong dilution effect on LV-OOA concentrations. In contrast to the LV-OOA, the diurnal variation of SV-OOA showed large concentration decease in the daytime, similar to that of nitrate, which should be the combined result of its semi-volatility and high PBL heights in the daytime.





ACPD
10, 25841–25869, 2010



### 3.5 Influence of meteorology on observed $PM_1$ components

Wind plays a crucial role in dilution and transport of air pollution, which is especially the case in this study since the Kaiping site is a rural site downwind of the polluted central PRD area. In order to better understand the origins of $PM_1$ at the Kaiping site, it is essential to study the relationship between the components concentrations and wind. Figure 7 plots the distribution of $PM_1$ component concentration versus wind direction and speed, which was mostly northeasterly during the sampling period in PRD. Generally, all the $PM_1$ components showed higher concentrations with lower wind speeds but lower concentrations with higher wind speeds, reflecting the vital role of wind in diluting air pollutants. The contrast, however, was not identical for different $PM_1$ components. Sulfate concentrations were maintained at medium levels even under higher wind speeds of >4 m/s, indicating that sulfate was a quite regional pollutant that dispersed more uniformly in PRD. For nitrate and chloride, their higher concentrations were constrained with weak winds (about <2 m/s), which implies either more local production or more gas-to-particle condensation at lower wind speeds. Considering Kaiping was a rural site with less local emissions, more gas-to-particle condensation of $HNO_3$ due to air pollutant accumulation under calm air conditions seems to be more plausible. Other $PM_1$ components had higher and relatively uniform concentrations associated with 0~4 m/s northeasterly wind, without even higher concentrations under weak winds (<2 m/s). This strongly suggests that regional transport from central PRD rather than local emission was the major origins of these $PM_1$ components at the Kaiping site.

## 4 Conclusions

A HR-ToF-AMS was deployed at a rural site downwind of the highly-polluted central PRD area to characterize submicron particles in the regional air during October–November 2008 as part of the STAR2008 PRD campaign. The $PM_1$ mass





ACPD
10, 25841–25869, 2010



concentrations in 10 min-resolution varied largely between 2.4 and 150 $\mu g\,m^{-3}$, with a mean value of 33.1 $\mu g\,m^{-3}$. Organics and sulfate were the most abundant components, accounting for 33.8% and 33.7% of the total $PM_1$ mass, respectively, followed by ammonium (14.0%), nitrate (10.7%), black carbon (6.7%), and chloride (1.1%) in sequence. The average size distributions of the species (excluding BC) were all dominated by an accumulation mode peaking at ~450 nm in $D_{va}$, indicating they were well internally mixed aged aerosols. Calculations of organic elemental composition based on the high-resolution organic mass spectra obtained indicate that C, H, O, and N on average contributed 56.6, 7.0, 35.1, and 1.3% to the total organic mass, respectively, which corresponds to an OM/OC ratio (the ratio of organic matter mass/organic carbon mass) of 1.77 ± 0.08. Positive Matrix Factorization (PMF) analysis on the high-resolution organic mass spectral dataset identified three organic components (BBOA, LV-OOA and SV-OOA), which on average accounted for 24.5, 39.6 and 35.8% of the total organic mass, respectively. The BBOA showed strong features of biomass burning emissions and its source was mainly attributed to the intensive field rice straw burning events after harvest, which increased the ambient loadings of organics and BC in $PM_1$ by 133% and 74%, respectively, compared to the non-burning time periods before the harvest. The LV-OOA and SV-OOA were revealed to correspond to more aged and fresher secondary organic aerosol, respectively. SV-OOA was found to correlate best with secondary nitrate while LV-OOA correlated best with secondary sulfate. Analysis of meteorological influence supported that regional transport from the central PRD area was the major origin of the $PM_1$ components observed at the Kaiping site.

**Supplementary material related to this article is available online at: http://www.atmos-chem-phys-discuss.net/10/25841/2010/acpd-10-25841-2010-supplement.pdf**.





ACPD
10, 25841–25869, 2010



*Acknowledgements.* This work was supported by the "863" project (2006AA06A308) from the Ministry of Science and Technology of China, the National Natural Science Funds for Distinguished Young Scholar (21025728) and the National Natural Science Foundation (40805049, 20777001) of China.

## References

Aiken, A. C., DeCarlo, P. F., and Jimenez, J. L.: Elemental analysis of organic species with electron ionization high-resolution mass spectrometry, Anal. Chem., 79, 8350–8358, 2007.

Aiken, A. C., Decarlo, P. F., Kroll, J. H., et al.: O/C and OM/OC ratios of primary, secondary, and ambient organic aerosols with high-resolution time-of-flight aerosol mass spectrometry, Environ. Sci. Technol., 42, 4478–4485, 2008.

Aiken, A. C., Salcedo, D., Cubison, M. J., Huffman, J. A., DeCarlo, P. F., Ulbrich, I. M., Docherty, K. S., Sueper, D., Kimmel, J. R., Worsnop, D. R., Trimborn, A., Northway, M., Stone, E. A., Schauer, J. J., Volkamer, R. M., Fortner, E., de Foy, B., Wang, J., Laskin, A., Shutthanandan, V., Zheng, J., Zhang, R., Gaffney, J., Marley, N. A., Paredes-Miranda, G., Arnott, W. P., Molina, L. T., Sosa, G., and Jimenez, J. L.: Mexico City aerosol analysis during MILAGRO using high resolution aerosol mass spectrometry at the urban supersite (T0) - Part 1: Fine particle composition and organic source apportionment, Atmos. Chem. Phys., 9, 6633–6653, doi:10.5194/acp-9-6633-2009, 2009.

Alfarra, M. R., Coe, H., Allan, J. D., et al.: Characterization of urban and rural organic particulate in the lower Fraser valley using two aerodyne aerosol mass spectrometers, Atmos. Environ., 38, 5745–5758, 2004.

Alfarra, M. R., Prevot, A. S. H., Szidat, S. et al.: Identification of the mass spectral signature of organic aerosols from wood burning emissions, Environ. Sci. Technol., 41, 5770–5777, 2007.

Allan, J. D., Alfarra,M. R., Bower, K. N., et al.: Quantitative sampling using an Aerodyne AerosolMass Spectrometer. Part 2: Measurements of fine particulate chemical composition in two UK Cities, J. Geophys. Res.-Atmos., 108, 4091, doi:10.1029/2002JD002359, 2003.

Canagaratna, M. R., Jayne, J. T., Jimenez, J. L., et al.: Chemical and microphysical characterization of ambient aerosols with the aerodyne aerosol mass spectrometer, Mass Spectrom. Rev., 26, 185–222, 2007.





ACPD

10, 25841–25869, 2010



de Gouw, J. A., Middlebrook, A. M., Warneke, C., et al.: Budget of organic carbon in a polluted atmosphere: results from the New England Air Quality Study in 2002, J. Geophys. Res.-Atmos., 110, D16305, doi:16310.11029/12004JD005623, 2005.

de Gouw, J. A., Warneke, C., Parrish, D. D., et al.: Emission sources and ocean uptake of acetonitrile ($CH_3CN$) in the atmosphere, J. Geophys. Res., 108(D11), 4329, doi:10.1029/2002JD002897, 2003.

DeCarlo, P. F., Kimmel, J. R., Trimborn, A., et al.: Field-Deployable, High-Resolution Time-of-Flight Aerosol Mass Spectrometer, Anal. Chem., 78, 8281–8289, 2006.

DeCarlo, P. F., Ulbrich, I. M., Crounse, J., de Foy, B., Dunlea, E. J., Aiken, A. C., Knapp, D., Weinheimer, A. J., Campos, T., Wennberg, P. O., and Jimenez, J. L.: Investigation of the sources and processing of organic aerosol over the Central Mexican Plateau from aircraft measurements during MILAGRO, Atmos. Chem. Phys., 10, 5257–5280, doi:10.5194/acp-10-5257-2010, 2010.

Docherty, K. S., Stone, E. A., Ulbrich, I. M., et al.: Apportionment of Primary and Secondary Organic Aerosols in Southern California during the 2005 Study of Organic Aerosols in Riverside (SOAR-1), Environ. Sci. Technol., 42, 7655–7662, 2008.

Drewnick, F., Hings, S. S., DeCarlo, P., et al.: A new time-of-flight aerosol mass spectrometer (TOF-AMS)-Instrument description and first field deployment, Aerosol. Sci. Tech., 39, 637–658, 2005.

Hagler, G. S. W., Bergin, M. H., Salmon, L. G., et al.: Source areas and chemical composition of fine particulate matter in the Pearl River Delta region of China, Atmos. Environ., 40, 3802–3815, 2006.

Han, S., Kondo, Y., Oshima, N., et al.: Temporal variations of elemental carbon in Beijing, J. Geophys. Res.-Atmos., 114, D23202, doi:10.1029/2009JD012027, 2009.

He, L.-Y., Lin, Y., Huang, X.-F., Guo, S., Xue, L., Su, Q., Hu, M., Luan, S.-J., and Zhang, Y.-H.: Characterization of high-resolution aerosol mass spectra of primary organic aerosol emissions from Chinese cooking and biomass burning, Atmos. Chem. Phys. Discuss., 10, 21237–21257, doi:10.5194/acpd-10-21237-2010, 2010.

Heald, C. L., Kroll, J. H., Jimenez, J. L., et al.: A simplified description of the evolution of organic aerosol composition in the atmosphere, Geophys. Res. Lett., 37, L08803, doi:10.1029/2010GL042737, 2010.

Hennigan, C. J., Sullivan, A. P., Fountoukis, C. I., Nenes, A., Hecobian, A., Vargas, O., Case Hanks, A. T., Huey, L. G., Lefer, B. L., Russell, A. G., and Weber, R. J.: On the volatility and





ACPD
10, 25841–25869, 2010



production mechanisms of newly formed nitrate and water soluble organic aerosol in Mexico City, Atmos. Chem. Phys. Discuss., 8, 4811–4829, doi:10.5194/acpd-8-4811-2008, 2008.
Hofzumahaus, A., Rohrer, F., Lu K., et al.: Amplified trace gas removal in the troposphere, Science, 324, 1702–1704, 2009.
Hua, W., Chen, Z. M., Jie, C. Y., Kondo, Y., Hofzumahaus, A., Takegawa, N., Chang, C. C., Lu, K. D., Miyazaki, Y., Kita, K., Wang, H. L., Zhang, Y. H., and Hu, M.: Atmospheric hydrogen peroxide and organic hydroperoxides during PRIDE-PRD'06, China: their concentration, formation mechanism and contribution to secondary aerosols, Atmos. Chem. Phys., 8, 6755–6773, doi:10.5194/acp-8-6755-2008, 2008.
Huang, X.-F., He, L.-Y., Hu, M., Canagaratna, M. R., Sun, Y., Zhang, Q., Zhu, T., Xue, L., Zeng, L.-W., Liu, X.-G., Zhang, Y.-H., Jayne, J. T., Ng, N. L., and Worsnop, D. R.: Highly time-resolved chemical characterization of atmospheric submicron particles during 2008 Beijing Olympic Games using an Aerodyne High-Resolution Aerosol Mass Spectrometer, Atmos. Chem. Phys., 10, 8933–8945, doi:10.5194/acp-10-8933-2010, 2010.
Huffman, J. A., Docherty, K. S., Aiken, A. C., Cubison, M. J., Ulbrich, I. M., DeCarlo, P. F., Sueper, D., Jayne, J. T., Worsnop, D. R., Ziemann, P. J., and Jimenez, J. L.: Chemically-resolved aerosol volatility measurements from two megacity field studies, Atmos. Chem. Phys., 9, 7161–7182, doi:10.5194/acp-9-7161-2009, 2009.
Jayne, J. T., Leard, D. C., Zhang, X. F., et al.: Development of an aerosol mass spectrometer for size and composition analysis of submicron particles, Aerosol. Sci. Tech., 33, 49–70, 2000.
Jimenez, J. L., Canagaratna, M. R., Donahue, N. M., et al.: Evolution of organic aerosols in the atmosphere, Science, 326, 1525–1529, 2009.
Jimenez, J. L., Jayne, J. T., Shi, Q., et al.: Ambient aerosol sampling using the Aerodyne Aerosol Mass Spectrometer, J. Geophys. Res.-Atmos., 108, 8425, doi:10.1029/2001JD001213, 2003.
Lanz, V. A., Alfarra, M. R., Baltensperger, U., Buchmann, B., Hueglin, C., and Prvt, A. S. H.: Source apportionment of submicron organic aerosols at an urban site by factor analytical modelling of aerosol mass spectra, Atmos. Chem. Phys., 7, 1503–1522, doi:10.5194/acp-7-1503-2007, 2007.
Lin, P., Hu, M., Deng, Z., et al.: Seasonal and diurnal variations of organic carbon in $PM_{2.5}$ in Beijing and the estimation of secondary organic carbon, J. Geophys. Res.-Atmos., 114, D00G11, doi:10.1029/2008JD010902, 2009.
Ng, N. L., Canagaratna, M. R., Zhang, Q., Jimenez, J. L., Tian, J., Ulbrich, I. M., Kroll, J. H.,





ACPD
10, 25841–25869, 2010



Docherty, K. S., Chhabra, P. S., Bahreini, R., Murphy, S. M., Seinfeld, J. H., Hildebrandt, L., Donahue, N. M., DeCarlo, P. F., Lanz, V. A., Prvt, A. S. H., Dinar, E., Rudich, Y., and Worsnop, D. R.: Organic aerosol components observed in Northern Hemispheric datasets from Aerosol Mass Spectrometry, Atmos. Chem. Phys., 10, 4625–4641, doi:10.5194/acp-10-4625-2010, 2010.

Paatero, P. and Hopke, P. K.: Discarding or downweighting high-noise variables in factor analytic models, Anal. Chim. Acta, 490, 277–289, 2003.

Paatero, P. and Tapper, U.: Positive Matrix Factorization–a Nonnegative Factor Model with Optimal Utilization of Error-Estimates of Data Values, Environmetrics, 5, 111–126, 1994.

Salcedo, D., Onasch, T. B., Dzepina, K., Canagaratna, M. R., Zhang, Q., Huffman, J. A., DeCarlo, P. F., Jayne, J. T., Mortimer, P., Worsnop, D. R., Kolb, C. E., Johnson, K. S., Zuberi, B., Marr, L. C., Volkamer, R., Molina, L. T., Molina, M. J., Cardenas, B., Bernab, R. M., Mrquez, C., Gaffney, J. S., Marley, N. A., Laskin, A., Shutthanandan, V., Xie, Y., Brune, W., Lesher, R., Shirley, T., and Jimenez, J. L.: Characterization of ambient aerosols in Mexico City during the MCMA-2003 campaign with Aerosol Mass Spectrometry: results from the CENICA Supersite, Atmos. Chem. Phys., 6, 925–946, doi:10.5194/acp-6-925-2006, 2006.

Streets, D., Yu, C., Bergin, M., et al.: Modeling study of air pollution due to the manufacture of export goods in China's Pearl River Delta, Environ. Sci. Technol., 40, 2099–2107, 2006.

Ulbrich, I. M., Canagaratna, M. R., Zhang, Q., Worsnop, D. R., and Jimenez, J. L.: Interpretation of organic components from Positive Matrix Factorization of aerosol mass spectrometric data, Atmos. Chem. Phys., 9, 2891–2918, doi:10.5194/acp-9-2891-2009, 2009.

Yuan, B., Liu, Y., Shao, M., et al.: Biomass Burning Contributions to Ambient VOCs Species at a Receptor Site in the Pearl River Delta (PRD), China, Environ. Sci. Technol., 44(12), 4577–4582, 2010.

Zhang, Q., Canagaratna, M. R., Jayne, J. T., et al.: Time- and size-resolved chemical composition of submicron particles in Pittsburgh: Implications for aerosol sources and processes, J. Geophys. Res.-Atmos., 110, D07S09, doi:10.1029/2004JD004649, 2005b.

Zhang, Q., Jimenez, J. L., Canagaratna, M. R., et al.: Ubiquity and dominance of oxygenated species in organic aerosols in anthropogenically-influenced Northern Hemisphere midlatitudes, Geophys. Res. Lett., 34, L13801, doi:10.1029/2007GL029979, 2007.

Zhang, Q., Worsnop, D. R., Canagaratna, M. R., and Jimenez, J. L.: Hydrocarbon-like and oxygenated organic aerosols in Pittsburgh: insights into sources and processes of organic aerosols, Atmos. Chem. Phys., 5, 3289–3311, doi:10.5194/acp-5-3289-2005, 2005.





ACPD
10, 25841–25869, 2010



Zhang, Y. H., Hu M., Zhong L. J., et al.: Regional Integrated Experiments on Air Quality over Pearl River Delta 2004 (PRIDE-PRD2004): Overview, Atmos. Environ., 42(25), 6157–6173, 2008.

Zheng, J., Zhang, R., Fortner, E. C., Volkamer, R. M., Molina, L., Aiken, A. C., Jimenez, J. L., Gaeggeler, K., Dommen, J., Dusanter, S., Stevens, P. S., and Tie, X.: Measurements of $HNO_3$ and $N_2O_5$ using ion drift-chemical ionization mass spectrometry during the MILAGRO/MCMA-2006 campaign, Atmos. Chem. Phys., 8, 6823–6838, doi:10.5194/acp-8-6823-2008, 2008.





ACPD

10, 25841–25869, 2010



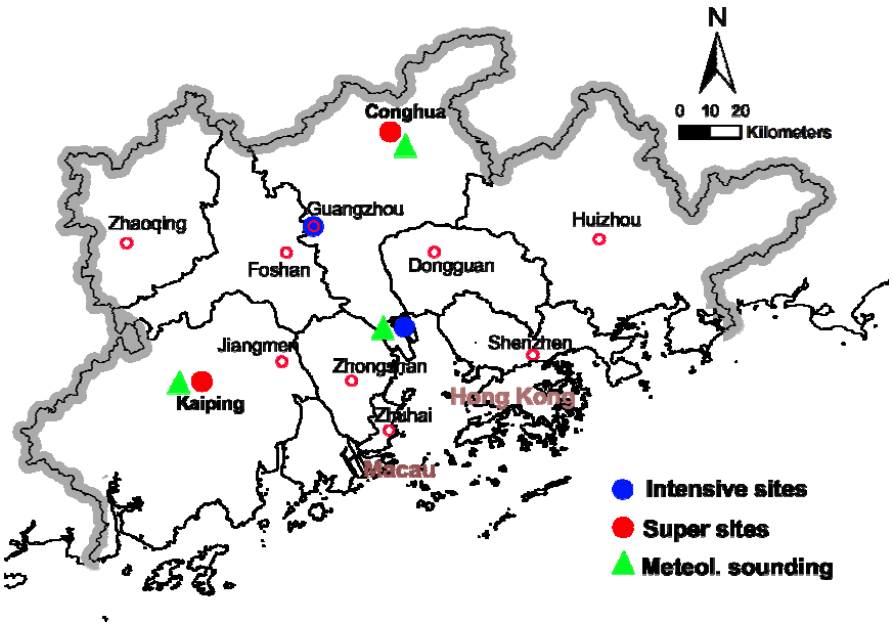


**Fig. 1.** The location of the Kaiping monitoring site in the PRD region.





ACPD
10, 25841–25869, 2010



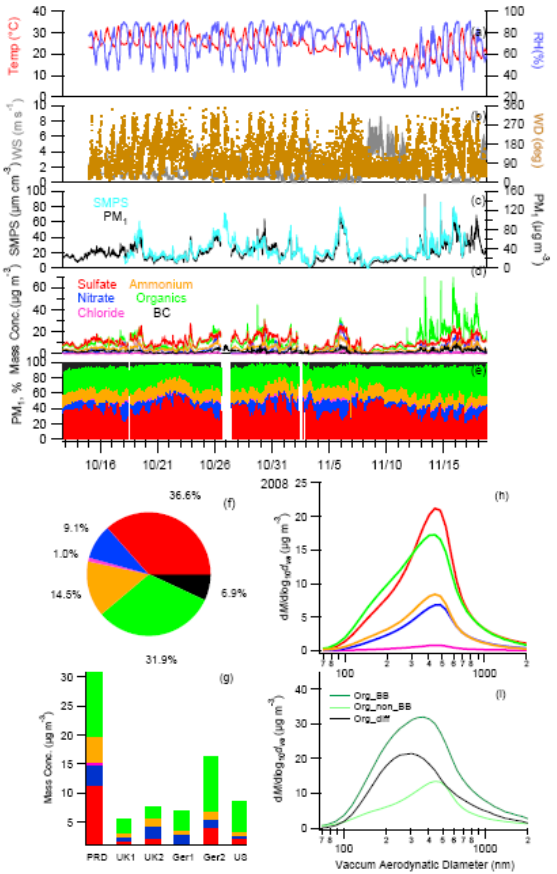


**Fig. 2.** The time series of **(a)** ambient temperature and relative humidity; **(b)** wind direction and wind speed; **(c)** $PM_1$ mass concentration by AMS species+BC and SMPS volume; **(d)** $PM_1$ species concentrations; **(e)** $PM_1$ percent composition; the average **(f)** $PM_1$ chemical composition; **(g)** comparison of species concentrations with other urban downwind sites; **(h)** mean species size distributions; and **(i)** mean OA size distributions during biomass burning period (after 12 November) and non-biomass burning period (before 12 November).





ACPD
10, 25841–25869, 2010



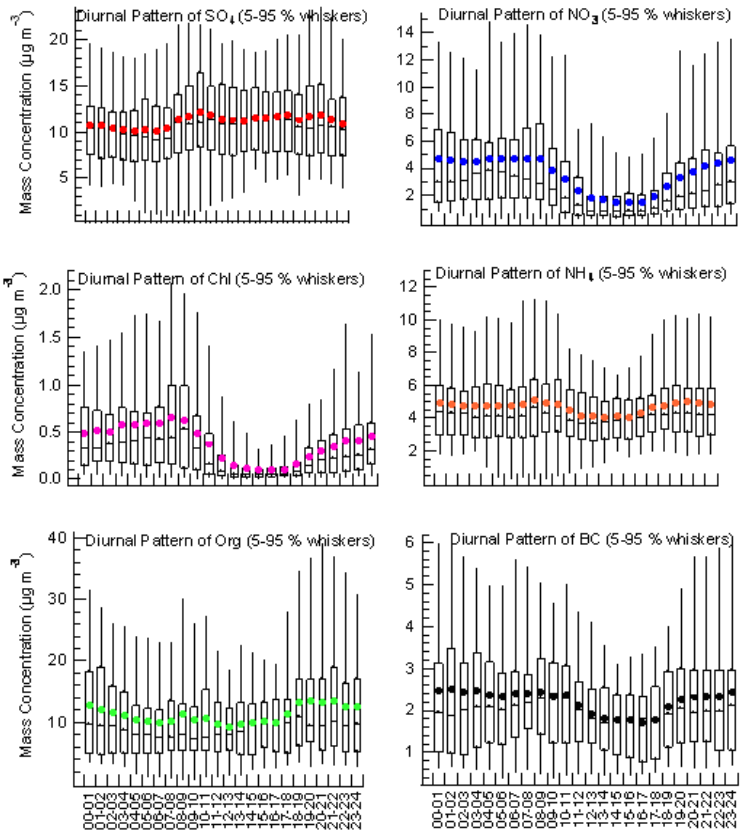


**Fig. 3.** Diurnal variation box plots of PM1 species. The upper and lower boundaries of boxes indicate the 75-th and 25-th percentiles; the line within the box marks the median; the whiskers above and below boxes indicate the 90-th and 10-th percentiles; and cross symbols represent the means.





ACPD
10, 25841–25869, 2010



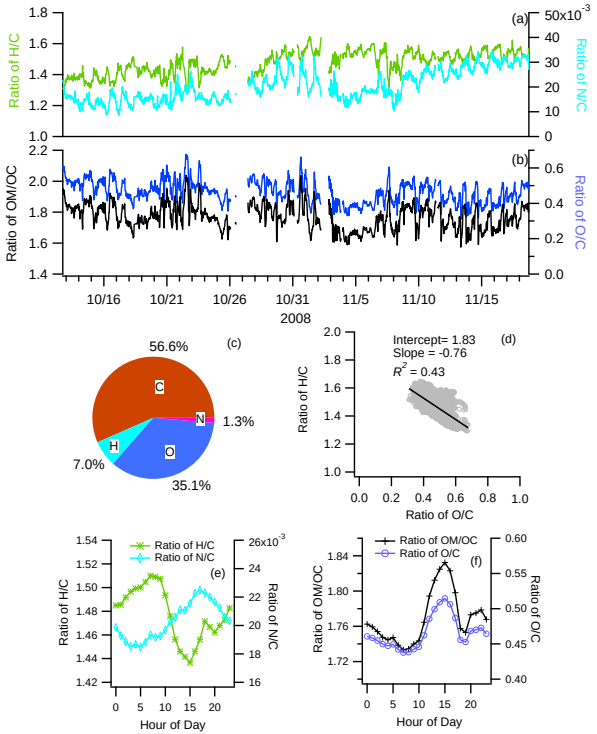


**Fig. 4.** The time series of **(a)** H/C and N/C ratios; and **(b)** O/C and OM/OC ratios; **(c)** the average mass-based organic elemental composition; **(d)** the Van Krevelen diagram (H/C versus O/C); the average diurnal variations of **(e)** H/C and N/C ratios and **(f)** O/C and OM/OC ratios.





ACPD
10, 25841–25869, 2010



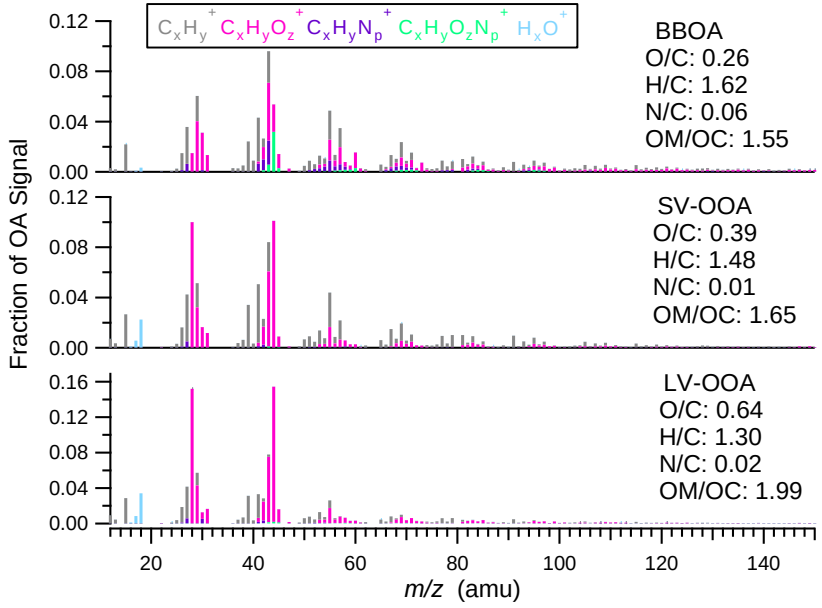


**Fig. 5.** The MS profiles of the three OA components identified by PMF in this study.





ACPD
10, 25841–25869, 2010



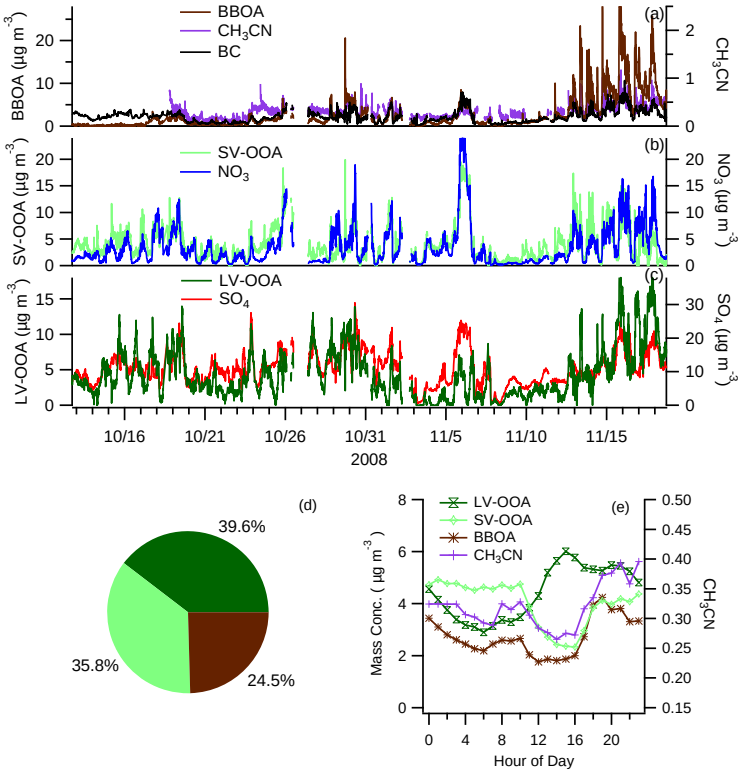


**Fig. 6.** Time series of **(ac)** the OA components and other relevant species; **(d)** the average OA composition; and **(e)** the diurnal variations of the OA components and acetonitrile.





ACPD
10, 25841–25869, 2010



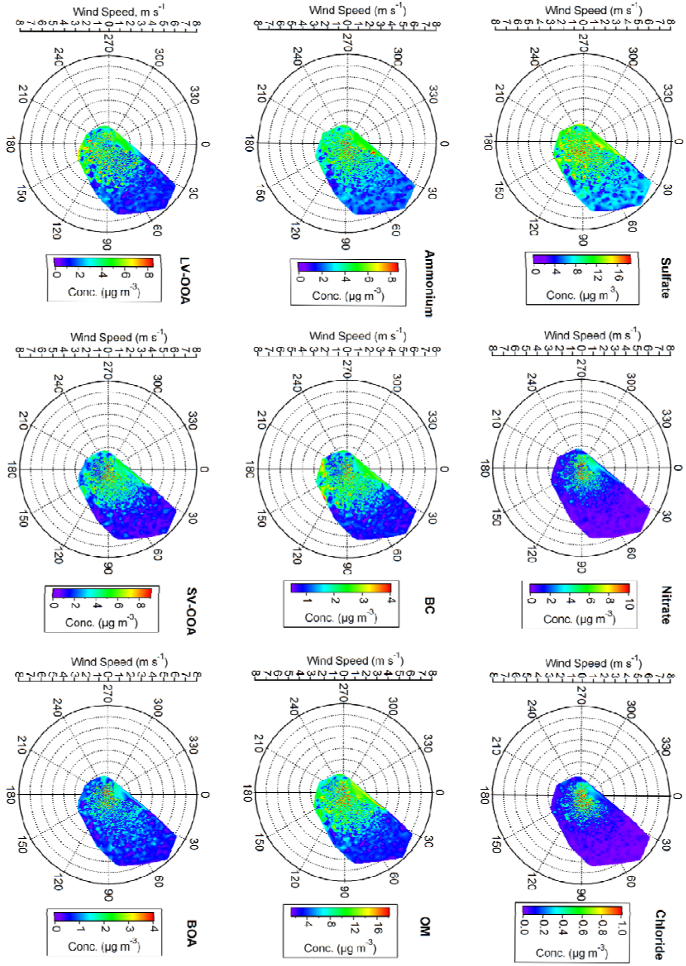


**Fig. 7.** The variation of $PM_1$ component concentration with wind direction and speed.





ACPD
10, 25841–25869, 2010

Characterization of submicron aerosols

X.-F. Huang et al.